https://doi.org/10.5194/egusphere-2025-5953
Preprint. Discussion started: 2 January 2026

Microwave Radiometry Improves Modelling of Surface Melt Processes of Antarctic Firn

Andreas Colliander[1,3], Nicole-Jeanne Schlegel[2], Alamgir Hossan[3], Catherine Walker[4], Joel Harper[5]

[1]Finnish Meteorological Institute, Helsinki, Finland
[2]NOAA/OAR Geophysical Fluid Dynamics Laboratory, Princeton, NJ, USA
[3]Jet Propulsion Laboratory, California Institute of Technology, Pasadena, CA, USA
[4]Woods Hole Oceanographic Institution, Woods Hole, MA, USA
[5]Geosciences, University of Montana, Missoula, MT, USA

Correspondence to: Andreas Colliander (andreas.colliander@fmi.fi)

Abstract. Surface melt strongly influences the thermodynamics and stability of Antarctic ice shelves, yet firn models remain poorly constrained due to scarce observations. We present a framework that integrates satellite-borne microwave radiometry with firn modelling to evaluate meltwater generation and infiltration. Using the Glacier Energy and Mass Balance (GEMB) surface energy balance model, we simulate snow and firn temperature, density, and liquid water content (LWC) on the Shackleton Ice Shelf. These outputs drive the Microwave Emission of Model of Layered Snowpacks (MEMLS) radiative transfer model to simulate microwave brightness temperatures (TB), which we compare with satellite radiometer observations at 1.4 and 36.5 GHz. Because TB is highly sensitive to LWC, this approach provides a powerful constraint on firn thermodynamics in data-sparse regions. Our results reveal that realistic simulation of meltwater percolation and refreezing requires substantially finer vertical resolution than typically employed. Incorporating radiometric constraints thus improves firn evolution modelling and advances projections of Antarctic ice shelf stability.

1 Introduction

The primary drivers of Antarctic Ice Sheet mass loss are basal melt and glacier outflow (Scambos et al., 2000; Bell et al., 2018). Ice shelves play a critical role in controlling glacier discharge, acting as barriers that regulate the flow of inland ice into the ocean (IPCC, 2021). Surface melt significantly impacts the long-term thermodynamics and structure of ice shelves, and thus their ability to buttress ice flow (e.g., DeConto and Pollard, 2016). During the austral summer, warmer air temperatures and increased solar radiation cause surface melting (e.g., Tedesco et al., 2007), most intensely on the more northerly latitudes, including the Antarctic Peninsula (Scambos et al., 2000), while southerly shelves such as the Ross and Filchner-Ronne experience melt more episodically (Banwell et al., 2021). Ice-shelf firn serves as a critical reservoir for meltwater that might otherwise pond on the surface and affect ice-shelf stability, ultimately influencing the flow of the inland ice sheet (e.g., Banwell et al., 2013; Bell et al., 2018). The meltwater percolates into the ice shelf, transforming its structural and thermal composition; the refrozen firn is left with reduced pore space available for meltwater retention,

https://doi.org/10.5194/egusphere-2025-5953
Preprint. Discussion started: 2 January 2026

potentially including ice lenses that block percolation and promote ponding (e.g., Dunmire et al., 2024). The ultimate infiltration of the water retained in the surface (ponding), controlled by the intensity and frequency of surface meltwater processes (e.g., Leeson et al., 2020), or seawater infiltrated into the ice shelves through basal crevasses, and their resulting structural changes, have been linked to calving and collapse events, such as the Larsen B collapse in 2002 (e.g., Scambos et al., 2003) and Conger-Glenzer in 2022 (e.g., Walker et al., 2024).

Because of their buttressing role, future ice sheet stability is tightly coupled to the health of the ice shelves (e.g., Fricker et al., 2025). Climate models, now beginning to incorporate coupled ice sheet-ocean interactions, are only just being evaluated for projections of sea-level change. Past assessments using one-way atmospheric and ocean forcing from Earth system models suggest that under high-emission scenarios, ice sheets could contribute substantially to sea level rise (IPCC, 2021). Yet predictions of ice shelf evolution remain under-constrained, as in situ measurements of melt and firn processes at scale are nearly impossible to acquire. Firn models struggle to represent liquid meltwater generation and evolution (e.g., Vandecrux et al., 2020) and depend on external forcing, energy-exchange parameterisation, and firn thermodynamics (Leeson et al., 2020). Their reliability is limited by reliance on model-based rather than observational data. Furthermore, firn model initial conditions, including density and thermal structure, are typically derived from spin-ups to mean historical states; errors in these profiles accumulate through each modelling cycle and affect infiltration and evolution. Combined with simplified process parameterisations, scarce observational validation, and frequent inter-model disagreement (e.g., Glaude et al., 2024), model fidelity remains highly uncertain.

The model shortcomings are particularly concerning when evaluating how increasing melt affects ice shelf stability. Accurate representation of liquid water content (LWC) and its distribution within ice shelves is crucial for reliable projections of ice mass loss. Misrepresentation of liquid water storage, refreezing, and percolation can bias model outputs and affect projections of sea-level contribution (Gilbert & Kittel, 2021). Failure to capture hydrofracturing and subsurface weakening – processes dependent on subsurface LWC – can lead to underestimates of sudden ice shelf collapse and glacier acceleration (Lai et al., 2020). Improved observational constraints, from both remote sensing and in situ measurements, are therefore essential for refining model processes and reducing uncertainty in long-term climate predictions (Rignot et al., 2019).

Microwave remote sensing provides a valuable tool for monitoring meltwater evolution and structural changes in ice shelves. Low-frequency emissions (e.g., 1.4 GHz) can originate from hundreds of meters within the ice shelf or the ice/seawater boundary (e.g., Leduc-Leballeur et al., 2015; Macelloni et al., 2016), and L-band radiometry has proven effective for capturing internal meltwater processes (Houtz et al., 2020; Leduc-Leballeur et al., 2020; Naderpour et al., 2021; Mousavi et al., 2021; 2022; Zieger et al., 2024). In contrast, higher frequency emissions (e.g., 37 GHz) are sensitive to near-surface conditions (e.g., Macelloni et al., 2007; Picard et al., 2022a) and have been used to assess ice shelf integrity and inform meltwater modelling (de Roda Husman et al., 2024; Zheng et al., 2022; 2025). While high frequencies provide binary surface information, total liquid water amount (LWA) and refreeze rates remain model-dependent and uncertain. Because lower-frequency signals retain sensitivity to larger-scale meltwater, combining multiple microwave bands offers

https://doi.org/10.5194/egusphere-2025-5953
Preprint. Discussion started: 2 January 2026

complementary insights into both shallow and deep ice-shelf processes (Colliander et al., 2022; 2023; Leduc-Leballeur et al., 2025).

LWA is a valuable metric for tracking firn evolution, capturing the interplay of meltwater generation and refreezing across diurnal, episodic, and seasonal scales. LWA retrievals from L-band radiometry agree well with values derived from surface energy balance models forced by reanalysis and in situ data (Hossan et al., 2024) and with subsurface temperature measurements (Moon et al., 2024), supporting both approaches. L-band observations also reflect vertical meltwater distribution, not just total LWA (Vandecrux et al., 2025; Moon et al., 2025). While dielectric mixing models of wet snow influence the magnitude of LWA retrievals, they do not alter observed trends in melt onset and cessation (Hossan et al., 2025). Although L-band brightness temperature (TB) can estimate LWA and percolation depth, physical models remain essential for simulating firn density, temperature, and structural integrity. Integrating observational and model-based approaches is therefore critical for understanding and projecting ice shelf evolution.

Here, we exploit this rapid evolution in understanding of 1.4 GHz radiometry, together with 36.5 GHz, to investigate the seasonal surface melt effects on the Shackleton Ice Shelf (SIS) over multiple seasons. We use modelled ice shelf physical information from the Ice-sheet and Sea-level System Model (ISSM) and the Glacier Energy and Mass Balance (GEMB) model (Gardner et al., 2023), together capturing the ice shelf structure as well as the snow and firn evolution, including its temperature, density, LWC, and other properties. The model is forced with the ERA5 (Hersbach et al., 2020). We then simulate TB at 1.4 and 36.5 GHz using the Microwave Emission of Layered Snowpacks (MEMLS) model (Wiesmann et al., 1999) and compare them to TB measured at 1.4 GHz by the NASA Soil Moisture Active Passive (SMAP) mission (Entekhabi et al., 2025) and at 36.5 GHz by the Advanced Microwave Scanning Radiometer 2 (AMSR2) instrument onboard the JAXA GCOM-W satellite (Imaoka et al., 2010). The GEMB model's ability to predict the LWC and firn evolution is tested during the seasonally occurring melt events at the SIS (e.g., de Roda Husman et al., 2023; Saunderson et al., 2022), model parameters are adjusted accordingly, and the forcing accuracy is assessed to improve the liquid water representation in the model.

2 Methods and Materials

2.1 Study Location: Shackleton Ice Shelf

Most of the Antarctic Ice Sheet (AIS) drains to the ocean, terminating in marine glacier cliffs, floating ice shelves, or glacier tongues (e.g., Rignot et al., 2011). Floating ice shelves and glaciers cover nearly two-thirds of the Antarctic coastline, an area comparable to the entire Greenland Ice Sheet (Rignot et al., 2013). Ice shelf mass loss occurs primarily via basal melting at the ice-ocean interface and iceberg calving, contributing roughly equally (Paolo et al., 2015; Rignot et al., 2013). The West Antarctic Ice Sheet (WAIS) has experienced significant mass loss since the 1990s, particularly in the Amundsen Sea sector (e.g., Smith et al., 2020). The East Antarctic Ice Sheet (EAIS), long considered more stable (Silvano et al., 2016) yet

https://doi.org/10.5194/egusphere-2025-5953
Preprint. Discussion started: 2 January 2026

containing almost 90% of Antarctica's sea-level equivalent (Fricker et al., 2025), is now also showing measurable but slower contributions to sea-level rise (Rignot et al., 2019).

Shackleton Ice Shelf, one of East Antarctica's largest ice shelf systems, fronts Queen Mary Land to the west and Wilkes Land's Knox Coast to the east. It is fed by several tributary glaciers, including Scott, Northcliff, Roscoe, Apfel, and Denman. The Denman Glacier alone is estimated to hold an ice mass equivalent to 1.5 m of sea level rise (Morlighem et al., 2020). The system comprises the Shackleton Ice Shelf itself, multiple pinning points, the ice tongues of Denman, Northcliff, Scott, and Roscoe, and an area of fast ice west of Denman's tongue that acts as a near-permanent seal to the main ice shelf (Figure S1). A major calving between 1997-2000 separated the Eastern Shackleton from what became the Conger-Glenzer Ice Shelf (Walker et al., 2024). The system features numerous rifts, including decades-old triple-junctions on its eastern front, and recent studies highlight active rift propagation, shear margin weakening, and surface features linked to brine infiltration.

2.2 Spaceborne Microwave Radiometer Data

We use L-band (1.4 GHz) TB from the SMAP radiometer operating in a 6 AM/PM equatorial crossing sun-synchronous orbit with 40° incidence angle, 38-km 3dB footprint, and 1000-km swath width (Piepmeier et al., 2017; Entekhabi et al., 2025), allowing the measurement of most of Antarctica twice daily. The SMAP science data production started on March 31, 2015. We used the spatially enhanced TB product (L1CTBE, version 3) posted to a consistent 9-km Equal-Area Scalable Earth grid version 2 (EASE2) polar grid (Brodzik et al., 2012; 2014; Chaubell et al., 2020).

We use Ka-band (36.5 GHz) TB from AMSR2, with a 1:30 AM/PM equatorial crossing sun-synchronous orbit (Imaoka et al., 2010). The 3dB footprint of the Ka-band channel is about ~8 km. The conically scanning, 55° incidence angle measurement results in ~1900 km swath width, overlapping with SMAP observations spatially and allowing the measurement of the entire Antarctica at least twice a day. The AMSR2 mission has produced science data since May 18, 2012. The data were gridded using inverse distance weighting on the same 9-km EASE2 grid as the SMAP data.

Lower frequencies (e.g., 1.4 GHz) originate from hundreds of meters within the ice shelf or the ice/sea-water boundary (e.g., Leduc-Leballeur et al., 2015; Macelloni et al., 2016), while higher frequency emissions (such as 36.5 GHz) are more sensitive to near-surface processes (e.g., Macelloni et al., 2007; Picard et al., 2022a; see also Figure S5), providing complementary insights into shallow and deep ice shelf processes (Colliander et al., 2022; 2023; Leduc-Leballeur et al., 2025). Data are analysed over the SIS study site (66.0782°S and 97.9590°E; Figure S1), where ICESat-2 shows uniform thickness, minimising any effects from the grounding line or pinning points on the radiometric signatures (Figure S2).

2.3 Glacier Energy and Mass Balance (GEMB)

We used the GEMB model to represent the snow, firn, and ice composition on the SIS. GEMB simulates glacier surface mass balance by accounting for energy exchanges at the snow–atmosphere interface (Gardner et al., 2023). It utilises temperature, radiation, wind speed, humidity, and precipitation inputs to compute surface melting, sublimation, and refreezing processes. The module calculates the energy available for melting based on net radiation, sensible, and latent heat

https://doi.org/10.5194/egusphere-2025-5953
Preprint. Discussion started: 2 January 2026

fluxes. This energy is then converted into meltwater production, contributing to surface runoff or refreezing within the snowpack. GEMB outputs detailed firn profiles, of which we used LWC, temperature, and density. Baseline simulations for Antarctica (1979-2023), including spin-up, were generated with GEMB in the ISSM (Gardner et al.,2023; Schlegel and Gardner, 2024). Our analysis uses the January 1, 2015, output nearest the SIS study location as the firn initial state. We then ran point simulations with MATLAB version of GEMB (Gardner, 2024) to 6 m depth using various layering schemes for 2015-2023, saving output at 3-hour intervals.

Two forcing datasets were utilised in the study. ERA5 reanalysis (Hersbach et al., 2020) provides a common option for Antarctic and Greenland simulations. We also used the automatic weather station at the Casey station (approx. 565 km east of SIS; Australian Antarctic Division, 2020) as a proxy for Shackleton conditions to estimate potential ERA5 biases and their effects on the GEMB simulations. The temperature differences between ERA5 and the station were calculated, with the station temperature adjusted by a lapse rate of -0.006K/m for elevation differences. The resulting bias was applied to GEMB temperature forcing, and downward long-wave radiation and saturation vapour pressure were adjusted accordingly, assuming unchanged near-surface emissivity and relative humidity.

The model generally uses thinner layers near the surface and thicker layers at depth, corresponding to decreasing vertical variability in snow, firn, and ice properties (Figure S4). The baseline layering scheme employed 5 cm layers down to 10 m, then increasing through the depth of the firn layer. To better capture highly variable melt-refreeze processes and their impact on microwave emission simulation, we also ran the model with thinner surface layers to the observed percolation depth (2-3 m), then increasing to 6 m. Configurations included 15, 10, 5, 2, and 1 mm constant layers to a depth of 3 m, as well as 1.5 mm and 1.25 mm down to a depth of 2.1 m, and 1 mm down to a depth of 2 m. The latter three simulations have shallower depths because the minimum surface layer depths must divide evenly, and they were much more resource-intensive to run. Results suggested that the modelled LWC in the snow converged between the 1 mm and 1.25 mm configurations. As a result, additional simulations were performed using the 1.25 mm surface layer thickness. Additional simulations included (1) running with a different thermal conductivity parameterization (i.e. Calonne et al., 2011), rather than the one used by the baseline simulation (i.e., Sturm et al., 1997), similar to experiments presented by Gardner et al., 2023, for Summit Station, Greenland, (2) running with the temperature bias derived from station data, and (3) running with the monthly climatological temperature bias derived from station data.

To simulate the ice properties below the firn layer, we use the ISSM. We calculate a three-dimensional thermal-mechanical steady-state solution of continental Antarctica with respect to the present-day climate, using GEMB temperatures at depth as the surface boundary condition of the dynamic incompressible ice. Results of this simulation are presented by Akins et al. (2025).

2.4 Brightness Temperature Modelling

We used the Microwave Emission Model of Layered Snowpacks (MEMLS; Weismann and Mätzler, 1999) to simulate TB over SIS at the 1.4 GHz (SMAP, 40° incidence) and the 36.5 GHz (AMSR2, 55° incidence). MEMLS is a radiative transfer

https://doi.org/10.5194/egusphere-2025-5953
Preprint. Discussion started: 2 January 2026

model that simulates microwave emission, absorption, and scattering in stratified snowpacks across a broad frequency range under varying snow and atmospheric conditions. It applies the six-flux approximation to compute radiation in each layer, allowing multiple scattering in both directions. Snow is represented as horizontally homogeneous layers defined by thickness, temperature, density, grain size (exponential correlation length, p_{ex}), and LWC. Layering, temperature, density, and LWC were taken directly from GEMB runs. A semi-infinite water layer with a dielectric constant of 80 (e.g., Ulaby et al., 1986) was assumed beneath the ice shelf, though contributing depth analysis showed negligible TB influence (Figure S5). Densification was handled through GEMB parameters without separate ice layers, as GEMB resolves snow/firn evolution through accumulation and melt-refreeze cycles (Figure S3). Since all top-layer thicknesses were less than a quarter of the wavelengths at 1.4 or 36.5 GHz, MEMLS was run in incoherent mode to properly account for scattering (Weissman and Mätzler, 1999).

The grain size tuning followed a widely used approach in snow simulations (e.g., Macelloni et al., 2007; Drinkwater et al., 2004). Grain size controls scattering in the Wiesmann et al. (1998) model used in MEMLS, which we applied consistently across all cases. We developed an empirical model function relating exponential correlation length (p_{ex}) to density and depth, tuning p_{ex} so that the simulated 1.4 and 36.5 GHz TB matched the frozen season observations. For 36.5 GHz, the function was further constrained (1) to reproduce the low TB caused by strong scattering from the surface crust formed after refreeze, and (2) to allow scattering effects to diminish over time, producing an increasing TB trend with snowpack evolution. The correlation length for the surface layers (up to about 1 m) took the following form:

$$p_1 = B_0 + A_0 e^{-z}\sqrt{\rho(z) - \rho_0} \quad (1)$$

where z is the depth, ρ density (kg/m^3), ρ_0 the new snow density, and A_0 and B_0 are the tuning parameters. B_0 is determined with pre-melt TB when fresh snow dominates the density profile in the upper 1 m (i.e., p_1 for fresh snow is B_0); A_0 is determined by the effect of the post-melt density spikes, and ρ_0 is close to fresh snow density, which is 450 kg/m^3 for Shackleton based on GEMB simulations.

For 1.4 GHz TB, the correlation length was modelled as:

$$p_2 = \phi\rho = A_\infty(1 - e^{-\alpha z})\rho \quad (2)$$

where the ϕ function links the density with grain size, and A_∞ and α are its tuning parameters. The measured TB is nearly constant throughout the frozen season, and the tuning was done using the same pre-melt date as for 36.5 GHz TB. The purpose of the exponentially decaying function toward the surface is to reduce the scattering effect of the density spikes in the surface, while utilising the physical-model-based density information from GEMB. The composite correlation length for the entire column was defined as:

$$p_{ex}(z) = \begin{cases} p_1, & \phi < \phi_0 \\ p_2, & \phi \geq \phi_0 \end{cases} \quad (3)$$

where ϕ_0 was determined so that the two frequencies are affected by the two grain size regimes separately, as tying the correlation length and density enabled the tuning for the two frequencies with the same profile (because the frequencies are sensitive to different depths).

https://doi.org/10.5194/egusphere-2025-5953
Preprint. Discussion started: 2 January 2026

Although the tuning is empirical, it has a physical interpretation. First, the frequency-dependent scattering coefficient of snow depends on density, grain size, and snow type, with uniformity of the medium also playing a role. Existing models capture scattering in low and high-density regimes, but intermediate densities remain challenging (Picard et al., 2022). Our formulation similarly introduces a switch-off depth for grain size, roughly separating the fresh annual accumulation (about 1 m based on ERA5) from the underlying multi-year snow, controlled by ϕ_0.

Second, L-band emission from deep layers is strongly influenced by firn structure. Multi-year firn, formed from surface snow undergoing annual melt-refreeze cycles, inevitably develops structural heterogeneity that GEMB cannot fully resolve. The observed low L-band TB is likely caused by internal reflection and scattering effects from this uneven stratigraphy (e.g., Jezek et al., 2022). Such effects can be modelled either by imposing strong density variability that enhances interlayer reflections (e.g., Brucker et al., 2011; Leduc-Leballeur et al., 2015; Macelloni et al., 2016) or by increasing scattering coefficients through large effective grain sizes without altering GEMB densities. Because MEMLS empirically tunes the exponential correlation length (grain size) to match observation, the precise grain size–scattering relationship is secondary. Eq. (2), which increases correlation length with depth and density, aligns with the dense-snow models that generally predict stronger scattering than low-density snow (e.g., Picard et al., 2022).

3 Results

3.1 Seasonality of Brightness Temperature Observations and Modelled Snow and Firn

SIS is a prime example of an ice shelf where surface melt strongly influences dynamics. Yet, there are no continuous ground observations to constrain climate models or validate snow/firn evolution. Modelling is therefore essential to assess its melt vulnerability. Figure 1a-d shows GEMB-modelled snow and firn evolution using two layering schemes: 5 cm layers to 10 m depth and 1.25 mm layers to 6 m (see Section 2.3). ERA5 air temperatures drive the first-layer snow temperature in GEMB, accounting for thermal conductivity and radiation effects, while ERA5 3-hourly and annual precipitation provide accumulation forcing. These inputs shape density in the top layers, capturing crust formation during melt-refreeze cycles and its burial under winter snowfall. GEMB's LWA further illustrates seasonal variations in LWA over SIS.

We found that the observed TB seasonality at 1.4 and 36.5 GHz aligns with GEMB simulations (Figure 1e). The two bands probe different depths: 1.4 GHz has a contributing depth of tens to hundreds of meters, while 36.5 GHz is limited to the top tens of centimetres (Figure S5). Consequently, their time series reflect different aspects of SIS evolution. The 1.4 GHz TB tracks total LWA, whereas the 36.5 GHz TB, sensitive to the surface, highlights periods of active meltwater production. Outside the austral summer, 1.4 GHz TB remains remarkably stable (e.g., Mousavi et al., 2022), with summer variability corresponding to year-to-year melt intensity. Warm and cold periods are marked in Figure 1 using 36.5 GHz TB from grounded ice upstream of the SIS grounding line, which remains melt-free. The consistently low background level arises from annual melt-refreeze layering, while summer increases correspond to the absorptive effects of wet snow.

https://doi.org/10.5194/egusphere-2025-5953
Preprint. Discussion started: 2 January 2026

The V- and H-pol 36 GHz TB follow a consistent annual cycle: high during wet-snow periods (due to absorption) and low during dry conditions within the contributing depth. Seasonal changes drive the low values, reaching a minimum at the end of the melt season and a maximum at the start. Refreezing of wet snow forms crusts that enhance scattering, producing very low TB. Fresh snow accumulation between melt seasons gradually buries these crusts, reducing scattering and raising TB. During the melt season, repeated melt-refreeze cycles grow crust layers, progressively increasing scattering and lowering the dry-condition TB.

Example GEMB profiles of snow and firn temperature, LWC, and density to 7 m depth from Dec 26, 2019 (early melt season) and Jan 15, 2020 (late melt season) highlight contrasting behaviours between the 1.25 mm and 5 cm layering schemes (Figure 2). A complete refreeze occurred between these dates. In the first event, both schemes produce similar temperature and LWC profiles, though the 1.25 mm scheme yields a denser surface and maintains higher density spikes from the two prior seasons, while the 5 cm scheme better preserves older-season spikes. Percolation depths are comparable in the first event but diverge sharply in the second: approx. 1.5 m for the 1.25 mm scheme versus only approx. 0.5 m for the 5 cm scheme, which also shows less total meltwater. Consequently, liquid water retention is longer in the 1.25 mm scheme, producing a closer match to the observed L-band signature (Figure 1d and e).

Melt-refreeze timing and wet-snow duration varied substantially from year to year, and results from the two-layering schemes were not always correlated. This outcome is expected for any firn model, given the lack of reliable references for meltwater production (due to uncertainties in the surface energy balance) and for percolation and refreeze (due to approximate infiltration physics and limited understanding of irreducible LWC, corrupting the thermal field). L-band TB, being directly sensitive to total LWA, provides a valuable constraint on both processes. In this case, the 1.25 mm scheme appears to capture reality more closely.

3.2 Comparing Observations with Model-based Brightness Temperature Simulations

We translated the GEMB-modelled ice shelf state into 1.4 and 36.5 GHz TB using MEMLS, allowing the observations to be used more directly to evaluate model performance and guide parameterisation. Direct TB simulations from firn models are rare, yet the firn model provides the necessary framework—layering, temperature, density, and LWC—for multilayer emission modelling. Snow grain size, however, was tuned as an effective parameter (e.g., Picard et al., 2022; see Section 2.4). Establishing robust links between firn models and radiative transfer simulations is critical for calibrating parameters, constraining their values, and paving the way for assimilation-based approaches.

The simulated L-band TB closely matches observations under both frozen and melt conditions (Figure 3). The frozen level is tuned, while MEMLS produces the melt values, with maxima slightly above 260 K. The 1.25 mm scheme aligns better with observed L-band TB during the 2019-2020 melt season, whereas melt effects were weaker in 2020-2021, with minimal differences between schemes. In 2019, both schemes captured the onset of melt, triggered by changes in surface energy balance. However, in January 2020, the model failed to reproduce observed diurnal melt-refreeze cycles seen at 36.5 GHz.

https://doi.org/10.5194/egusphere-2025-5953
Preprint. Discussion started: 2 January 2026

Adjusting ERA5 forcing using Casey Station observations, its climatology, and incremental warming did not resolve the discrepancy, pointing instead to issues in model setup, spin-up, calibration, or parameterisation.

Refreezing all liquid water to complete the melt season depends on the end of new meltwater generation and the refreeze rate. In the 1.25 mm GEMB simulation, TB returned to frozen levels in late February 2020, whereas L-band observations refreezing completed in early March 2020. The forcing adjustments did not resolve this mismatch either, again pointing to shortcomings in GEMB.

The simulated 36.5 GHz TB reproduces both melt (approx. 273 K) and frozen states, including the frozen TB decrease from crust accumulation. Early in the season, the 1.25 mm and 5 cm schemes produced similar results due to the comparable LWC, but differences emerged later as their LWC diverged. In most cases, the 1.25 mm scheme captured melt events missed by the 5 cm scheme. For example, on February 20, 2020, the 5 cm case showed warming in the top layer but no melt, whereas the 1.25 mm case reproduced the observed melt and matched 36.5 GHz TB. However, on some days, the 1.25 mm scheme overestimated TB.

LWA retrieved from 1.4 GHz TB using the algorithm of Hossan et al. (2024) is shown in Figure 3e. In summer 2020, the retrieval and GEMB both indicate the melt onset, but their evolution differs: the retrieval shows persistent liquid water throughout the season, consistent with observed TB (Figure 3a), whereas GEMB produced episodic melt events tied to air temperature and surface energy balance (Figure 3d). In summer 2021, melt was weaker, with retrieved LWA not exceeding 10 mm; here, GEMB captured the timing and magnitude reasonably well. While subject to its own uncertainties – from footprint heterogeneity to electromagnetic model assumptions – the retrieval highlights gaps in how firn models represent meltwater and thermodynamic processes across different settings.

4 Discussion and Conclusion

By directly linking observations and simulations, the simulated TB provides a powerful constraint on meltwater generation, refreezing, and LWA across different model configurations. This establishes TB as a calibration reference and reframes Antarctic surface melt modelling. The approach builds on recent advances in utilising the lower-frequency passive microwave spectrum to capture meltwater-related emissions (Houtz et al., 2020; Mousavi et al., 2020; Hossan et al., 2024; Moon et al., 2024; Vandecrux et al., 2025). In the absence of in situ data, such observations fill a critical gap. Although widespread implementation remains technically demanding, it is warranted by the critical need to integrate observational constraints into firn models. Because these models underpin the conversion of surface altimetry into mass balance estimates and inform projections of ice sheet evolution, improving their representation of melt processes—central to ice shelf thermodynamics and stability—has the potential to enhance the long-term climate and sea-level hindcasts and forecasts significantly. When comparing simulated and observed TB from June 2015 to July 2021, winter values spread with accumulation, while melt events cluster near 270 K at 36.5 GHz (Figure S6). Deviations outside this range highlight missed or falsely predicted melt. At 1.4 GHz, the scatter in Figure S6 is dominated by melt events that the model fails to capture.

https://doi.org/10.5194/egusphere-2025-5953
Preprint. Discussion started: 2 January 2026

The residuals – observed minus simulated TB – provide a foundation for future data assimilation to constrain models better, improving performance.

Our results suggest that accurately modelling melt on the SIS may require layering as fine as 1.25 mm. By contrast, most state-of-the-art models employ much coarser layers (≥10 cm), which miss key processes such as liquid water generation, its percolation, retention, and refreezing, and ice layer formation. These processes are singularly transformative for the firn properties at depth, including temperature and density. Observations further show that in cold, episodic-melt environments, liquid water can persist at shallow depths. Coarse vertical resolution fails to capture these dynamics, compromising energy exchange and phase change representation and propagating errors into simulations under warm conditions.

The formation of high-density ice layers through refreezing and their control on subsequent meltwater infiltration and retention are highly sensitive to model resolution. Whether and how thick such layers form determines permeability and depends on how well the vertical structure is represented. Fine layering offers the most accurate depiction but is computationally expensive, requiring many layers with short time steps to maintain numerical stability. A balance is therefore needed between fidelity and efficiency (e.g., Gardner et al., 2023). Observations, such as LWA and infiltration depth (Vandecrux et al., 2025; Moon et al., 2025), could inform these choices, enabling adaptive schemes that dynamically adjust layer resolution in response to evolving liquid water and firn conditions.

Without observational constraints, firn models typically initialise from climatological spin-ups (e.g., 1950–1980), yet the thermal and density structure—particularly its spatial and vertical heterogeneity—strongly controls infiltration and firn evolution. Errors in these initial states propagate forward, biasing outcomes. Radiometric modelling offers a direct means to constrain firn thermal and density profiles from satellite observations, a critical step for next-generation modelling. No matter how advanced a melt or infiltration scheme may be, if it operates on a misrepresented firn column, predictions will diverge from reality over time. Our results highlight the high-impact potential of integrating radiometric data into firn models to improve model constraints, calibration, and initialisation, ultimately enhancing projections of Antarctic ice shelf stability, mass balance, and sea-level rise.

https://doi.org/10.5194/egusphere-2025-5953
Preprint. Discussion started: 2 January 2026

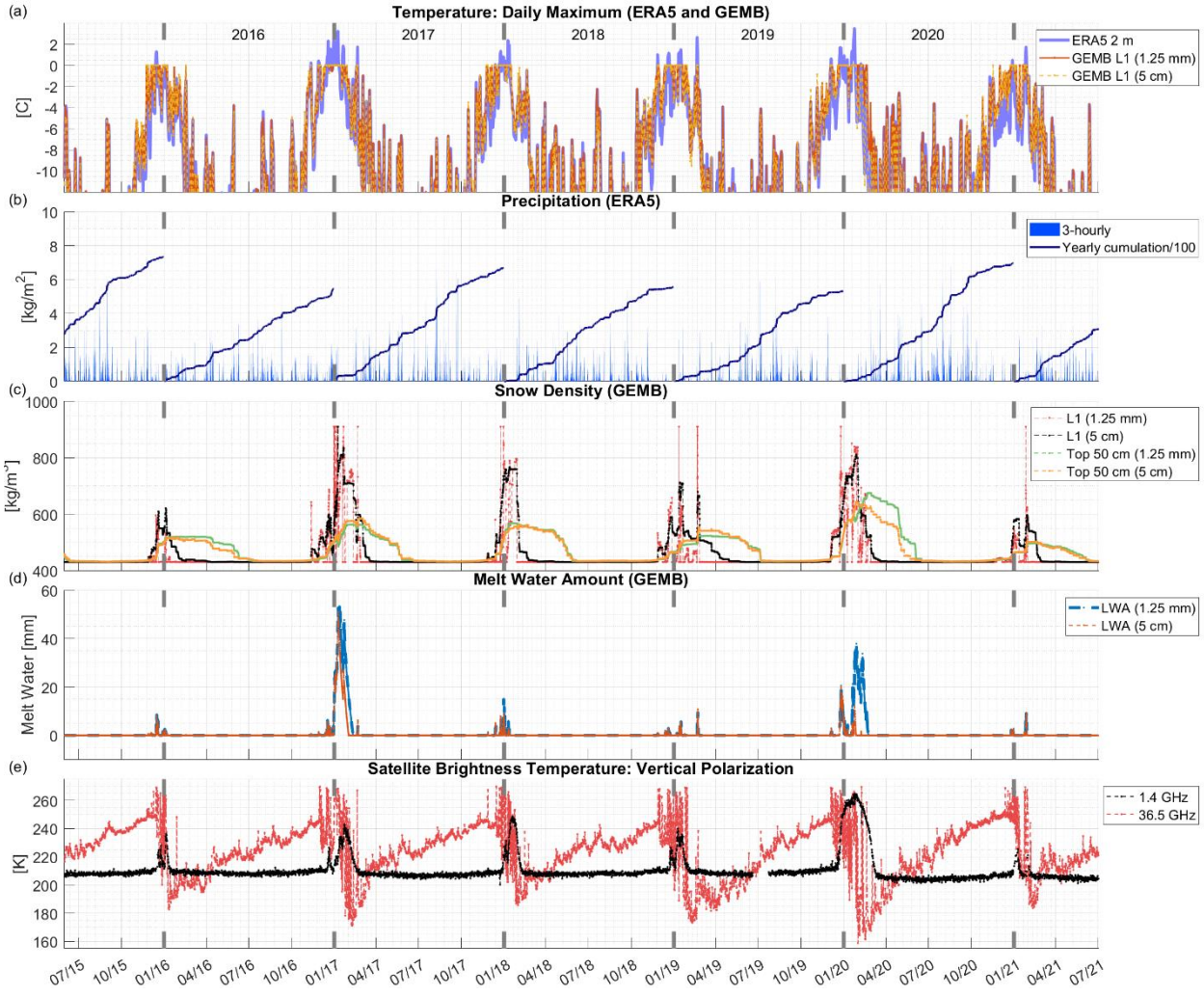

Figure 1. Modelled and measured parameters over the Shackleton Ice Sheet study location from July 2015 to July 2021. (a) ERA5 air temperature, GEMB layer 1 (L1) snow temperature for the 1 mm and 5 cm layering schemes. (b) The 3-hourly ERA5 precipitation (snow) and its yearly accumulation. (C) GEMB layer 1 snow density for the 1 mm and 5 cm layering schemes and the average snow density in the top 50 cm for the 1 mm and 5 cm layering schemes. (d) GEMB meltwater amount for the 1 mm and 5 cm layering schemes. (e) Measured 1.4 GHz (SMAP) and 36.5 GHz (AMSR2) brightness temperatures (TB).

https://doi.org/10.5194/egusphere-2025-5953
Preprint. Discussion started: 2 January 2026

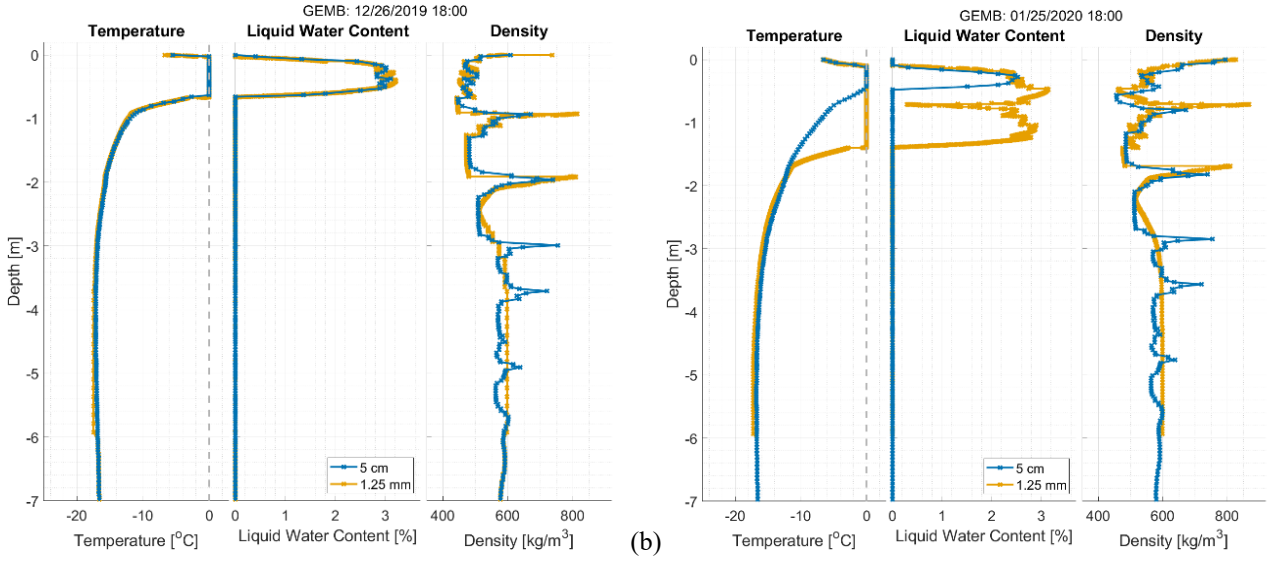

Figure 2. Temperature, liquid water content, and density depth profiles for the Shackleton Ice Shelf modelled with GEMB with 5 cm and 1.25 mm layers: a) early melt season on December 26, 2019, and b) later in the melt season on January 25, 2020.

https://doi.org/10.5194/egusphere-2025-5953
Preprint. Discussion started: 2 January 2026

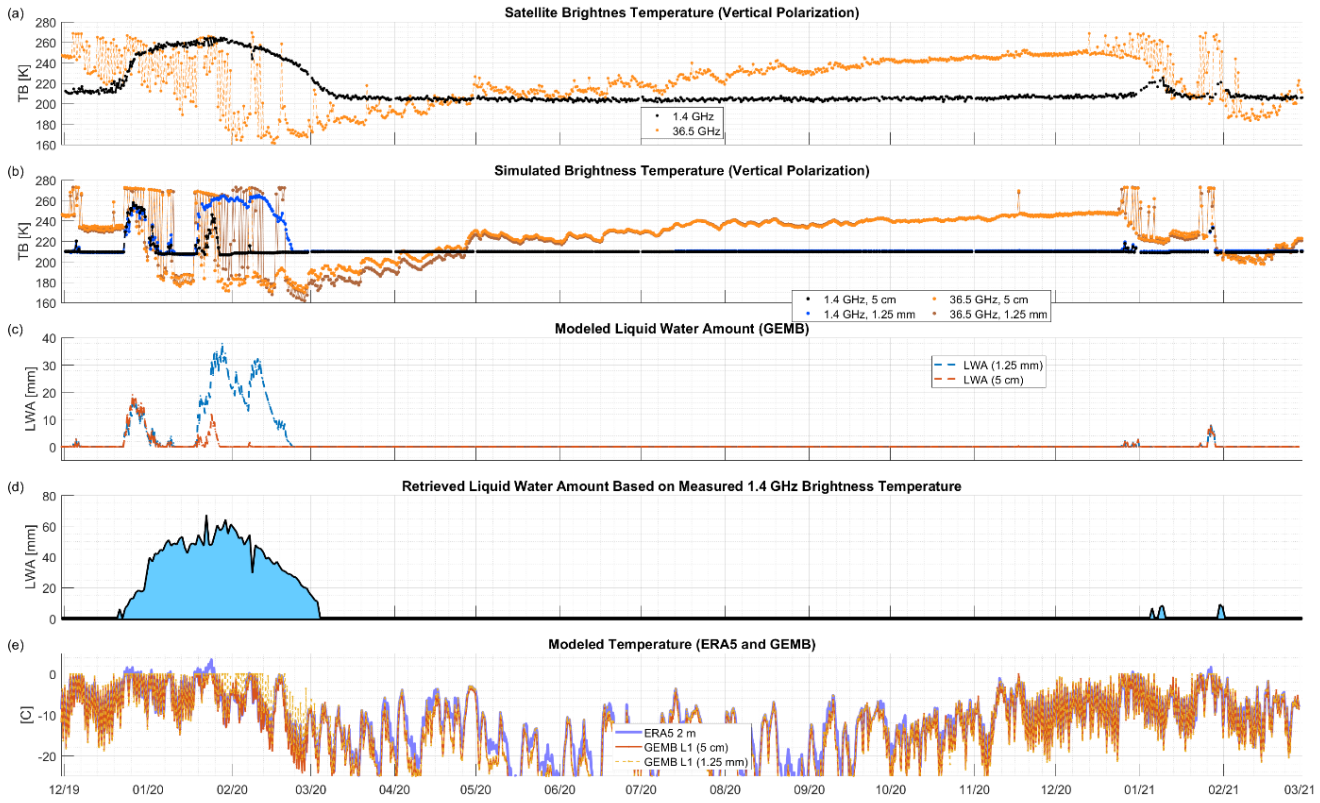

Figure 3. Measured, simulated, and modelled parameters for the study location at Shackleton ice shelf from December 2019 to March 2021. (a) Vertically polarised brightness temperature (TB) measured by SMAP and AMSR2 satellite radiometers at 1.4 and 36.5 GHz, respectively (the same as Figure 1 (e) but highlighting the shorter period). (b) Simulated 1.4 and 36.5 GHz TB using the physical representation of the ice shelf by GEMB and the MEMLS microwave emission model. (c) Liquid water amount by GEMB (the same as Figure 1 (d) but highlighting the shorter period). (d) Liquid water amount retrieved from the SMAP 1.4 GHz TB using the algorithm described in Hossan et al. (2024). (e) The 3-hourly ERA5 air temperature, GEMB layer 1 (L1) snow temperature for the 1 mm and 5 cm layering schemes.

Acknowledgements

This work was conducted in part at the Jet Propulsion Laboratory, California Institute of Technology, under a contract with the National Aeronautics and Space Administration. The authors gratefully acknowledge computational resources and support from the NASA Advanced Supercomputing Division. During the preparation of this work, the authors used Grammarly and ChatGPT to improve the language and readability; after using the tools, the authors reviewed and edited the content as needed and take full responsibility for the content of the publication. The data used in the study are available at figshare (Colliander et al., 2025).

https://doi.org/10.5194/egusphere-2025-5953
Preprint. Discussion started: 2 January 2026

Code/Data availability

The data is available at Colliander et al. (2025).

Author contribution

AC designed the study, generated the MEMLS model runs, analysed the modelled results and satellite measurements, and led the manuscript writing. NJS generated the GEMB model runs and contributed to study design, interpretation of results, and manuscript editing. AH supported the MEMLS model setup and execution, data processing, validation, and contributed to manuscript editing. CW provided the ice-shelf thickness analysis and other ice-shelf-specific information and contributed to interpretation, contextual analysis, and manuscript editing. JH contributed to interpretation, contextual analysis, and manuscript editing. All authors reviewed and approved the final manuscript.

Competing interests

There are no competing interests.

References

Akins, A. B., Tanner, A. B., Colliander, A., Schlegel, N.-J., Boudad, K., Yanovsky, I., Brown, S. T., & Misra, S. (2025). A Sparse Synthetic Aperture Radiometer Constellation Concept for Remote Sensing of Antarctic Ice Sheet Temperature. IEEE Transactions on Geoscience and Remote Sensing, 63, 1–21. https://doi.org/10.1109/tgrs.2025.3534466

Australian Antarctic Division. Casey research station. Australian Antarctic Program. Australian Government — Department of Climate Change, Energy, the Environment and Water (updated 15 September 2020). Available at: https://www.antarctica.gov.au/antarctic-operations/stations-and-field-locations/casey/

Ashcraft, I. S., & Long, D. G. (2006). Observation and characterization of radar backscatter over Greenland. IEEE Transactions on Geoscience and Remote Sensing, 44(11), 2940–2949. doi:10.1109/TGRS.2006.881106

Banwell, A. F., MacAyeal, D. R., & Sergienko, O. V. (2013). Breakup of the Larsen B Ice Shelf triggered by chain reaction drainage of supraglacial lakes. Geophysical Research Letters, 40(22), 5872–5876. doi: 10.1002/2013gl057694

Banwell, A. F., Datta, R. T., Dell, R. L., Moussavi, M. S., Brucker, L., Picard, G., & Tedesco, M. (2021). The 32-year record-high surface melt in 2019/2020 on the northern George VI Ice Shelf, Antarctic Peninsula. The Cryosphere, 15(2), 909–925. doi:10.5194/tc-15-909-2021

Bell, R. E., Banwell, A. F., Trusel, L. D., & Kingslake, J. (2018). Antarctic surface hydrology and impacts on ice-sheet mass balance. Nature Climate Change, 8(12), 1044–1052. doi:10.1038/s41558-018-0230-4

https://doi.org/10.5194/egusphere-2025-5953
Preprint. Discussion started: 2 January 2026

Brucker, L., Picard, G., Arnaud, L., Barnola, J.-M., Schneebeli, M., Brunjail, H., Lefebvre, E., & Fily, M. (2011). Modeling time series of microwave brightness temperature at Dome C, Antarctica, using vertically resolved snow temperature and microstructure measurements. Journal of Glaciology, 57(201), 171–182. https://doi.org/10.3189/002214311795306736

Calonne, N., Flin, F., Morin, S., Lesaffre, B., du Roscoat, S. R., and Geindreau, C.: Numerical and experimental investigations of the effective thermal conductivity of snow, Geophys. Res. Lett., 38, L23501, https://doi.org/10.1029/2011GL049234, 2011.

Colliander, A., Mousavi, M., Kimball, J. S., Miller, J. Z., & Burgin, M. (2023). Spatial and temporal differences in surface and subsurface meltwater distribution over Greenland ice sheet using multi-frequency passive microwave observations. Remote Sensing of Environment, 295, 113705. https://doi.org/10.1016/j.rse.2023.113705

Colliander, A., Mousavi, M., Marshall, S., Samimi, S., Kimball, J. S., Miller, J. Z., Johnson, J., & Burgin, M. (2022). Ice Sheet Surface and Subsurface Melt Water Discrimination Using Multi-Frequency Microwave Radiometry. Geophysical Research Letters, 49(4). https://doi.org/10.1029/2021gl096599

Colliander, A., Schlegel, N.-J., Hossan, A., Walker, C., & Harper, J. (2025). Microwave Radiometry Improves Modeling of Antarctic Surface Melt Processes: Data [Dataset]. figshare. https://doi.org/10.6084/M9.FIGSHARE.30052789

de Roda Husman, S. de R., Hu, Z., Wouters, B., Munneke, P. K., Veldhuijsen, S., & Lhermitte, S. (2023). Remote Sensing of Surface Melt on Antarctica: Opportunities and Challenges. IEEE Journal of Selected Topics in Applied Earth Observations and Remote Sensing (Vol. 16, pp. 2462–2480). https://doi.org/10.1109/jstars.2022.3216953

de Roda Husman, S., Lhermitte, S., Bolibar, J., Izeboud, M., Hu, Z., Shukla, S., van der Meer, M., Long, D., & Wouters, B. (2024). A high-resolution record of surface melt on Antarctic ice shelves using multi-source remote sensing data and deep learning. Remote Sensing of Environment, 301, 113950. https://doi.org/10.1016/j.rse.2023.113950

Drinkwater, M. R., Floury, N., & Tedesco, M. (2004). L-band ice-sheet brightness temperatures at Dome C, Antarctica: spectral emission modelling, temporal stability and impact of the ionosphere. Annals of Glaciology, 39, 391–396. https://doi.org/10.3189/172756404781814014

Dunmire, D., Wever, N., Banwell, A. F., & Lenaerts, J. T. M. (2024). Antarctic-wide ice-shelf firn emulation reveals robust future firn air depletion signal for the Antarctic Peninsula. Communications Earth & Environment, 5(1). doi: 10.1038/s43247-024-01255-4

Entekhabi, D., S. Yueh, R. Bindlish, M. Garcia, J. Entin, A. Colliander, M. J. Chaubell, W. Crow, R. Scott Dunbar, L. Herwehe, J. Kimball, P.N. Mohammed, R. Reichle, N. Chung, E. Dinnat, H. Huang, et al. (2025). The NASA Soil Moisture Active Passive (SMAP) Earth Observation Satellite Mission. IEEE Proceedings, Under Review.

Fricker, H.A. et al. (2025), Antarctica in 2025: Drivers of deep uncertainty in projected ice loss. Science, 387, 601-609. DOI:10.1126/science.adt9619

https://doi.org/10.5194/egusphere-2025-5953
Preprint. Discussion started: 2 January 2026

Galton-Fenzi, B. K., Fricker, H. A., Bassis, J. N., Crawford, A. J., Gomez, N., & Schoof, C. (2025). The Antarctic Ice Sheet and Sea Level. In Antarctica and the Earth System (pp. 141–163). Routledge. https://doi.org/10.4324/9781003406471-7

Gardner, A. S., Schlegel, N.-J., & Larour, E. (2023). Glacier Energy and Mass Balance (GEMB): a model of firn processes for cryosphere research. Geoscientific Model Development (Vol. 16, Issue 8, pp. 2277–2302). https://doi.org/10.5194/gmd-16-2277-2023

Gardner, A. (2024). alex-s-gardner/GEMB: GEMB v1.0 (Version v1.0). Zenodo. https://doi.org/10.5281/ZENODO.12534194

Gilbert, E., & Kittel, C. (2021). Surface melt and liquid water retention in the Antarctic ice sheet inferred from regional climate modeling. The Cryosphere, 15(2), 571–593. doi:10.5194/tc-15-571-2021

Glaude, Q., Noel, B., Olesen, M., Van den Broeke, M., van de Berg, W. J., Mottram, R., Hansen, N., Delhasse, A., Amory, C., Kittel, C., Goelzer, H., & Fettweis, X. (2024). A Factor Two Difference in 21st-Century Greenland Ice Sheet Surface Mass Balance Projections From Three Regional Climate Models Under a Strong Warming Scenario (SSP5-8.5). Geophysical Research Letters, 51(22). https://doi.org/10.1029/2024gl111902

Hersbach, H., Bell, B., Berrisford, P., Hirahara, S., Horányi, A., Muñoz-Sabater, J., Nicolas, J., Peubey, C., Radu, R., Schepers, D., Simmons, A., Soci, C., Abdalla, S., Abellan, X., Balsamo, G., Bechtold, P., Biavati, G., Bidlot, J., Bonavita, M., et al. (2020). The ERA5 global reanalysis. Quarterly Journal of the Royal Meteorological Society (Vol. 146, Issue 730, pp. 1999–2049). https://doi.org/10.1002/qj.3803

Hossan, A., Colliander, A., Vandecrux, B., Schlegel, N.-J., Harper, J., Marshall, S., & Miller, J. Z. (2024). Retrieval and Validation of Total Seasonal Liquid Water Amounts in the Percolation Zone of Greenland Ice Sheet Using L-band Radiometry. https://doi.org/10.5194/egusphere-2024-2563

Hossan, A., Colliander, A., Schlegel, N.-J., Harper, J., Andrews, L., Kolassa, J., Miller, J. Z., and Cullather, R.: Evaluation of Wet Snow Dielectric Mixing Models for L-Band Radiometric Measurement of Liquid Water Content in Greenland's Percolation Zone, EGUsphere [preprint], https://doi.org/10.5194/egusphere-2025-2681, 2025.

Imaoka, K., M. Kachi, H. Fujii, H. Murakami, M. Hori, A. Ono, T. Igarashi, K. Nakagawa, T. Oki, Y. Honda, and H. Shimoda (2010). Global Change Observation Mission (GCOM) for Monitoring Carbon, Water Cycles, and Climate Change. IEEE Proc., Vol. 98, No. 5, pp. 717-734.

Intergovernmental Panel on Climate Change (IPCC). (2021). Summary for Policymakers. In V. Masson-Delmotte et al. (Eds.), Climate Change 2021: The Physical Science Basis. Contribution of Working Group I to the Sixth Assessment Report of the Intergovernmental Panel on Climate Change. Cambridge University Press. doi:10.1017/9781009157896.002

Jezek, K. C., Wang, S., Leduc-Leballeur, M., Johnson, J. T., Brogioni, M., Miller, J. Z., Long, D. G., & Macelloni, G. (2022). Relationships Between L-Band Brightness Temperature, Backscatter, and Physical Properties of the Ross Ice

https://doi.org/10.5194/egusphere-2025-5953
Preprint. Discussion started: 2 January 2026

Shelf Antarctica. IEEE Transactions on Geoscience and Remote Sensing, 60, 1–14. https://doi.org/10.1109/tgrs.2022.3218538

Lai, C. Y., Kingslake, J., Wearing, M. G., Chen, P. H. C., Gentine, P., Li, H., & Spergel, J. J. (2020). Vulnerability of Antarctic ice shelves to meltwater-driven fracturing. Nature, 584(7822), 574–578. doi:10.1038/s41586-020-2627-8

Leduc-Leballeur, M., Picard, G., Mialon, A., Arnaud, L., Lefebvre, E., Possenti, P., & Kerr, Y. (2015). Modeling L-Band Brightness Temperature at Dome C in Antarctica and Comparison With SMOS Observations. IEEE Transactions on Geoscience and Remote Sensing (Vol. 53, Issue 7, pp. 4022–4032). https://doi.org/10.1109/tgrs.2015.2388790

Leduc-Leballeur, M., Picard, G., Macelloni, G., Mialon, A., & Kerr, Y. H. (2020). Melt in Antarctica derived from Soil Moisture and Ocean Salinity (SMOS) observations at L band. The Cryosphere (Vol. 14, Issue 2, pp. 539–548). https://doi.org/10.5194/tc-14-539-2020

Leduc-Leballeur, M., Picard, G., Zeiger, P., and Macelloni, G.: Empirical classification of dry-wet snow status in Antarctica using multi-frequency passive microwave observations, EGUsphere [preprint], https://doi.org/10.5194/egusphere-2025-732, 2025.

Leeson, A. A., Forster, E., Rice, A., & Gourmelen, N. (2020). Evolution of supraglacial lakes on the Greenland Ice Sheet. The Cryosphere, 14(2), 481–490. doi:10.5194/tc-14-481-2020

Macelloni, G., Brogioni, M., Pampaloni, P., & Cagnati, A. (2007). Multifrequency Microwave Emission Fromthe Dome-C Area on the East Antarctic Plateau: Temporal and Spatial Variability. IEEE Transactions on Geoscience and Remote Sensing (Vol. 45, Issue 7, pp. 2029–2039). https://doi.org/10.1109/tgrs.2007.890805

Macelloni, G., et al. (2011). Technical Support for the Deployment of an L-band Radiometer at Concordia Station During DOMEX-2 and Data Analysis. Final Report. Version 2.0. October 2011. European Space Agency Stify Contract Reports. https://earth.esa.int/eogateway/documents/20142/37627/DOMEX-2-Final-Report.pdf

Macelloni, G., Leduc-Leballeur, M., Brogioni, M., Ritz, C., & Picard, G. (2016). Analyzing and modeling the SMOS spatial variations in the East Antarctic Plateau. Remote Sensing of Environment (Vol. 180, pp. 193–204). https://doi.org/10.1016/j.rse.2016.02.037

Mätzler, C., & Wiesmann, A. (1999). Extension of the Microwave Emission Model of Layered Snowpacks to Coarse-Grained Snow. Remote Sensing of Environment, 70(3), 317–325. https://doi.org/10.1016/s0034-4257(99)00047-4

Moon, T., Harper, J., Colliander, A., Hossan, A., & Humphrey, N. (2024). L-Band Radiometric Measurement of Liquid Water in Greenland's Firn: Comparative Analysis with In Situ Measurements and Modeling. California Digital Library (CDL). https://doi.org/10.31223/x56712

Moon, T., J. Harper, A. Colliander, A. Hossan. (2025). Depth of Liquid Water Infiltration in Greenland Firn based on L-band Radiometry, a Snow Physics Model, and Machine Learning. Under Review.

Montomoli, F., Brogioni, M., Macelloni, G., Leduc-Leballeur, M., Baldi, M., Martin-Neira, M., & Casal, T. G. D. (2022). Long Term L-Band Brightness Temperature of the DOMEX-3 Experiment: Improvement of Absolute Calibration and

https://doi.org/10.5194/egusphere-2025-5953
Preprint. Discussion started: 2 January 2026

Data Analysis. IGARSS 2022 - 2022 IEEE International Geoscience and Remote Sensing Symposium (pp. 7367–7370). https://doi.org/10.1109/igarss46834.2022.9883561

Morlighem, M., Rignot, E., Binder, T., Blankenship, D., Drews, R., Eagles, G., Eisen, O., Ferraccioli, F., Forsberg, R., Fretwell, P., Goel, V., Greenbaum, J. S., Gudmundsson, H., Guo, J., Helm, V., Hofstede, C., Howat, I., Humbert, A., Jokat, W., … Young, D. A. (2019). Deep glacial troughs and stabilizing ridges unveiled beneath the margins of the Antarctic ice sheet. Nature Geoscience, 13(2), 132–137. https://doi.org/10.1038/s41561-019-0510-8

Mousavi, M., Colliander, A., Miller, J., & Kimball, J. S. (2022). A Novel Approach to Map the Intensity of Surface Melting on the Antarctica Ice Sheet Using SMAP L-Band Microwave Radiometry. IEEE Journal of Selected Topics in Applied Earth Observations and Remote Sensing, 15, 1724–1743. https://doi.org/10.1109/jstars.2022.3147430

Naderpour, R., Houtz, D., & Schwank, M. (2020). Snow wetness retrieved from close-range L-band radiometry in the western Greenland ablation zone. Journal of Glaciology (Vol. 67, Issue 261, pp. 27–38). https://doi.org/10.1017/jog.2020.79

Paolo, F. S., Fricker, H. A., & Padman, L. (2015). Volume loss from Antarctic ice shelves is accelerating. Science, 348(6232), 327–331. https://doi.org/10.1126/science.aaa0940

Picard, G., Leduc-Leballeur, M., Banwell, A. F., Brucker, L., & Macelloni, G. (2022a). The sensitivity of satellite microwave observations to liquid water in the Antarctic snowpack. The Cryosphere, 16(12), 5061–5083. https://doi.org/10.5194/tc-16-5061-2022

Picard, G., Löwe, H., & Mätzler, C. (2022b). Brief communication: A continuous formulation of microwave scattering from fresh snow to bubbly ice from first principles. The Cryosphere, 16(9), 3861–3866. https://doi.org/10.5194/tc-16-3861-2022

Rignot, E., Jacobs, S., Mouginot, J., & Scheuchl, B. (2013). Ice-Shelf Melting Around Antarctica. Science, 341(6143), 266–270. https://doi.org/10.1126/science.1235798

Rignot, E., Mouginot, J., & Scheuchl, B. (2011). Ice Flow of the Antarctic Ice Sheet. Science, 333(6048), 1427–1430. https://doi.org/10.1126/science.1208336

Rignot, E., Mouginot, J., Scheuchl, B., van den Broeke, M., van Wessem, J. M., & Morlighem, M. (2019). Four decades of Antarctic ice sheet mass balance from 1979–2017. Proceedings of the National Academy of Sciences, 116(4), 1095–1103. doi:10.1073/pnas.1812883116

Scambos, T. A., Hulbe, C., Fahnestock, M., & Bohlander, J. (2000). The link between climate warming and break-up of ice shelves in the Antarctic Peninsula. Journal of Glaciology, 46(154), 516–530. doi:10.3189/172756500781833043

Scambos, T., Hulbe, C., & Fahnestock, M. (2003). Climate-induced ice shelf disintegration in the Antarctic Peninsula. Antarctic Research Series (pp. 79–92). doi: 10.1029/ar079p0079

Schlegel, N.-J., & Gardner, A. (2024). Output from the Glacier Energy and Mass Balance (GEMB v1.0) forced with 3-hourly ERA5 fields and gridded to 10km, Greenland and Antarctica 1979-2023 (1.3-5day) [Data set]. Zenodo. https://doi.org/10.5281/zenodo.10806250

https://doi.org/10.5194/egusphere-2025-5953
Preprint. Discussion started: 2 January 2026

Silvano, A., Rintoul, S., & Herraiz-Borreguero, L. (2016). Ocean-Ice Shelf Interaction in East Antarctica. Oceanography, 29(4), 130–143. https://doi.org/10.5670/oceanog.2016.105

Smith, B., Fricker, H. A., Gardner, A. S., Medley, B., Nilsson, J., Paolo, F. S., Holschuh, N., Adusumilli, S., Brunt, K., Csatho, B., Harbeck, K., Markus, T., Neumann, T., Siegfried, M. R., & Zwally, H. J. (2020). Pervasive ice sheet mass loss reflects competing ocean and atmosphere processes. Science, 368(6496), 1239–1242. https://doi.org/10.1126/science.aaz5845

Sturm, M., Holmgren, J., König, M., and Morris, K.: The thermal conductivity of seasonal snow, J. Glaciol., 43, 26–41, 1997.

Tedesco, M., Abdalati, W., & Zwally, H. J. (2007). Persistent surface snowmelt over Antarctica (1987–2006) from 19.35 GHz brightness temperatures. Geophysical Research Letters (Vol. 34, Issue 18). https://doi.org/10.1029/2007gl031199

Ulaby, F. T., Moore, R. K., & Fung, A. K. (1986). Microwave Remote Sensing: Active and Passive. Volume III: From Theory to Applications. Artech House, Norwood, MA.

Vandecrux, B., Mottram, R., Langen, P. L., Fausto, R. S., Olesen, M., Stevens, C. M., Verjans, V., Leeson, A., Ligtenberg, S., Kuipers Munneke, P., Marchenko, S., van Pelt, W., Meyer, C. R., Simonsen, S. B., Heilig, A., Samimi, S., Marshall, S., Machguth, H., MacFerrin, M., et al. (2020). The firn meltwater Retention Model Intercomparison Project (RetMIP): evaluation of nine firn models at four weather station sites on the Greenland ice sheet. The Cryosphere (Vol. 14, Issue 11, pp. 3785–3810). https://doi.org/10.5194/tc-14-3785-2020

Vandecrux, B., G. Picard, P. Zeiger, M. Leduc-Leballeur, A. Colliander, A. Hossan, A. Ahlstrøm. (2025). Estimating the depth of subsurface water on the Greenland Ice Sheet using multi-frequency passive microwave remote sensing, radiative transfer modeling, and machine learning. Remote Sensing of Environment, Under Review.

Walker, C. C., Millstein, J. D., Miles, B. W. J., Cook, S., Fraser, A. D., Colliander, A., Misra, S., Trusel, L. D., Adusumilli, S., Roberts, C., & Fricker, H. A. (2024). Multi-decadal collapse of East Antarctica's Conger–Glenzer Ice Shelf. Nature Geoscience (Vol. 17, Issue 12, pp. 1240–1248). https://doi.org/10.1038/s41561-024-01582-3

Wiesmann, A., Mätzler, C., & Weise, T. (1998). Radiometric and structural measurements of snow samples. Radio Science, 33(2), 273–289. https://doi.org/10.1029/97rs02746

Wiesmann, A., & Mätzler, C. (1999). Microwave Emission Model of Layered Snowpacks. Remote Sensing of Environment (Vol. 70, Issue 3, pp. 307–316).. https://doi.org/10.1016/s0034-4257(99)00046-2